Activity-dependent COX-2 proteolysis generates a catalytically inactive fragment that affects aerobic respiration

Liat Hartal Benishay[1], Sharon Tal[1], Amal Abd Elkader[1], Omar Ehsainieh[1], Ranin Srouji-Eid[1], Martin Mikl[1], and Liza Barki-Harrington[1, *]

[1] Department of Human Biology, Faculty of Natural Sciences, University of Haifa, Haifa, Israel.

* Correspondence: Lbarki@psy.haifa.ac.il

Keywords: Cyclooxygenase-2 (COX-2), PTGS2, arachidonic acid, enzymatic activity, suicide inactivation, fatty acids, proteolysis, protease, mitochondria, lactate.

Summary

Cyclooxygenase-2 (COX-2) catalyzes arachidonic acid (AA) into PGH_2, the single source of all prostaglandins (PGs), ligands that activate multiple inflammatory pathways. AA catalysis by COX-2 quickly leads to suicide inactivation, rendering the enzyme catalytically inactive. We show that the catalytic activity is followed by controlled cleavage of COX-2, an event that is differentially regulated by fatty acids and blocked by COX inhibitors. Using mass spectrometry, we identified two adjacent cleavage points within the catalytic domain, which give rise to COX-2 fragments that are catalytically-inactive and localize to different cellular compartments. RNA-seq analysis revealed that one of these fragments significantly alters the expression of genes in the mitochondrial electron transport chain. Subsequent functional assays confirmed that cells expressing this fragment exhibit reduced mitochondrial function and increased lactate production. Our results suggest that in addition to its role in generating PGs, COX-2 has a subsequent, PG-independent function that emanates from its proteolysis.

Graphical Abstract

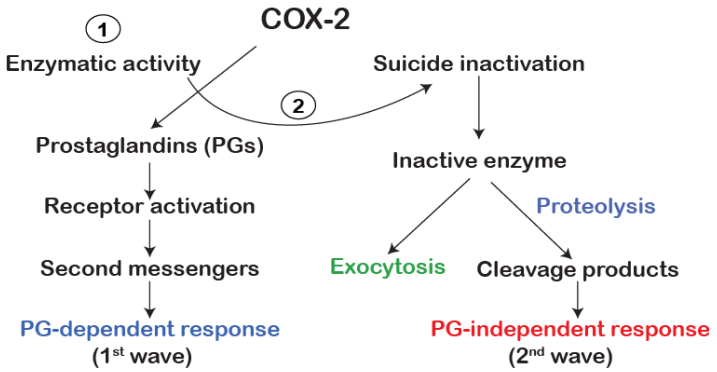

Introduction

Cyclooxygenase-2 (COX-2) is an enzyme that catalyzes the rate-limiting step in the conversion of arachidonic acid (AA) to prostaglandins (PGs) – bioactive lipids that play central roles in inflammation. Except for several tissues where it is constitutively expressed (*e.g.* kidney, brain), COX-2 expression is usually low, and its levels are rapidly upregulated in response to a wide range of inflammatory and pathological signals, thus producing the PGs that mediate a major part of inflammation [1].

COX-2 converts AA into prostaglandin H_2 (PGH_2), the source of all subsequent PGs, by a two-step redox reaction, which occurs in the catalytic domain of the protein [2,3]. The COX-2 enzyme is an obligatory dimer, consisting of two identical monomers, each containing the same active site for AA catalysis. However, only one of the two active sites catalyzes AA [4,5], while the other serves as an allosteric modulator of the active site. The rate of catalysis is affected by fatty acids, non-steroidal anti-inflammatory drugs (NSAIDs), and selective COX-2 inhibitors that either compete with AA in the catalytic site or modulate its activity by binding to the allosteric site [6-9].

Free radicals formed during catalysis cause COX-2 to quickly become catalytically inactive, by a mechanism of substrate-dependent suicide inactivation [2,3,10]. Interestingly, whereas the cellular proteasome regularly degrades the quiescent COX-2 that has not been exposed to AA, the fate of the catalytically inactive protein is largely unknown [11,12]. We have previously shown that some of the substrate-inactivated COX-2 is discarded from the cells by exosomes [13]. Now we show that AA-stimulation also causes the COX-2 protein to undergo limited proteolysis and that some of the resulting fragments inhibit aerobic respiration in a PG-independent manner.

Results

A fragment of COX-2 appears following its stimulation with AA

We have previously shown that a brief stimulation of HEK 293 cells overexpressing COX-2 with AA, causes the appearance of a smaller COX-2 immunoreactive band of ~40 kD [13]. To determine whether this is a general phenotype of COX-2, we stimulated multiple human cancer-derived cell lines with endogenous COX-2 expression, with AA, and probed the samples with an anti-COX-2 antibody directed against the N-terminal of the protein. As depicted in Fig. 1A, AA stimulation caused the appearance of a ~40 KD COX-2 immunoreactive band in all cell lines examined. Some cells (e.g. A549, HeLa, MCF10A) also expressed additional COX-2 immunoreactive bands that were less affected by the presence of AA. An immunoreactive band of the same size was also observed after AA stimulation in the murine-derived RAW 264.7 macrophages (Fig. 1B) and in HEK 293 cells with exogenous expression of COX-2 (Fig. 1C).

Together, these data suggest that the AA-dependent appearance of the lower COX-2 immunoreactive band is a general phenomenon that is not restricted to a certain cell line or species or to whether COX-2 is endogenously or ectopically- expressed.

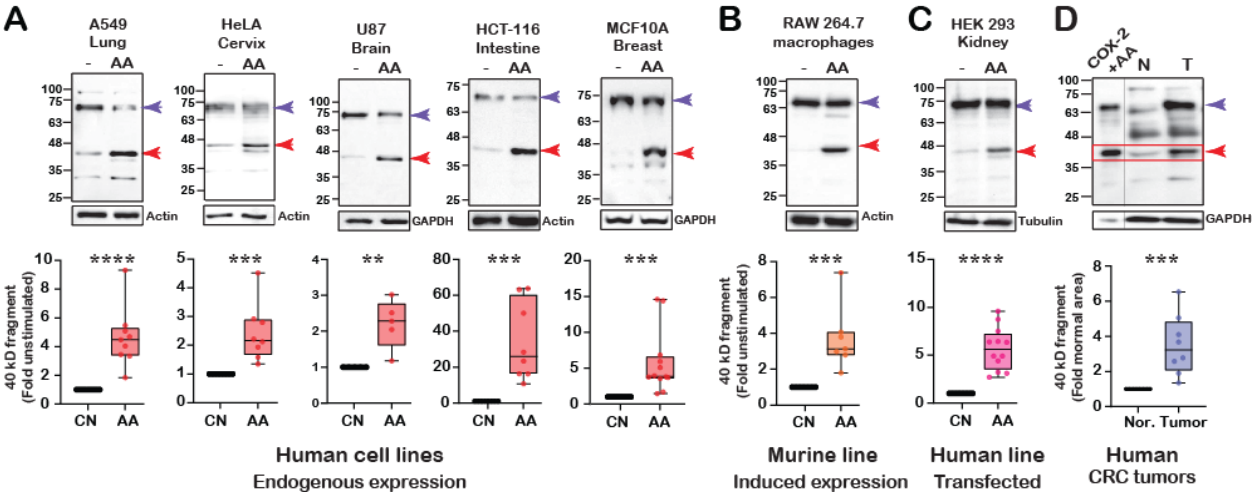

Fig. 1: A fragment of COX-2 appears following its stimulation with AA

(A) Representative western blots (upper panels) and quantification (lower panels) of data from five human cancer-derived cell lines with endogenous COX-2 expression, before and after stimulation with arachidonic acid (AA). A549 (n=9), HeLa (n=8), U87 (n=5), HCT-116 (n=8), and MCF10A (n=11).

(B) Representative western blots (upper panel) and quantification (lower panel) of data from murine RAW 264.7 cells, with overnight LPS-induced COX-2 expression, before and after stimulation with AA (n=6).

(C) Representative western blots (upper panel) and quantification (lower panel) of data from COX-2 transfected HEK 293 cells, before and after stimulation with AA (n=12).

(D) Representative samples from a tumor (T) and surrounding normal tissues (N) obtained from a colorectal cancer patient, ran alongside a sample of COX-2 expressing HEK 293 cells stimulated with AA, and quantification of n=8 samples. Statistical analysis was performed using the Wilcoxon test.

Quantification of the protein levels of the COX-2 fragment was done after normalization by GAPDH or actin. Data are represented as mean ± SD. Statistical significance was assessed by Student's t-test. $^{*}p < 0.05$, $^{**}p < 0.01$, $^{***}p < 0.001$, and $^{****}p < 0.0001$.

We next examined the expression of COX-2 in a small cohort of eight samples of colorectal tumors of patients diagnosed with low or moderate colorectal adenocarcinoma [14]. As depicted in Fig. 1D, cancerous samples also showed elevated expression of a ~40 kD immunoreactive band compared to tissue obtained from the clean margins of the same sample. This fragment was the same size as the one that appeared in AA-stimulated COX-2 expressing cells (Fig. 1D, lane 1). While the sample size of the patient cohort is too small to make any meaningful correlations with the pathology of the disease, its severity, or prognosis, these findings suggest that smaller COX-2 fragments exist in vivo, and hence support the rationale for searching for their identity and possible function in the cell.

The appearance of the COX-2 fragment requires enzymatic activity

Following binding to COX-2, AA is catalyzed in two structurally and functionally interconnected sites. The first is a cyclooxygenase (COX) reaction, which takes place in a hydrophobic channel in the core of the enzyme where prostaglandin endoperoxide G_2 (PGG_2) is generated. The subsequent peroxidase (POX) reaction occurs at a heme-containing active site located near the protein surface where PGG_2 is reduced to PGH_2. Specific PG synthases then catalyze PGH_2 into PGs (PGE_2, PGD_2, PGI_2, $PGF_{1\alpha}$) and thromboxane (TXA_2) all of which activate multiple signaling pathways by binding to G protein-coupled receptors [2,15]. To determine which of these stages is necessary for AA-mediated generation of the COX-2 fragment, we first tested whether the final products of AA catalysis can cause the appearance of this band. For this, we treated COX-2-expressing cells with PGE_2, one of the most abundant products of AA catalysis, for 30-120 min. As depicted in Fig. 2A, in contrast to AA stimulation, PGE_2 treatment did not cause the appearance of the COX-2 fragment, suggesting that this phenomenon is probably not mediated by the soluble products of AA catalysis.

Since the appearance of the COX-2 fragment was dependent upon the presence of AA, we next pretreated the cells with reversible or irreversible inhibitors of COX-2 (ibuprofen and aspirin, respectively) before stimulation with AA. The results presented in Fig. 2B-D show that treatment with both compounds blocked the appearance of the COX-2 fragment. Ibuprofen and aspirin both inhibit catalytic activity by preventing access of AA to the catalytic sites [2]. We therefore postulated that the generation of the COX-2 fragment requires either binding and/or catalytic processing of AA. A productive binding mode of AA to the enzyme is obtained when it is positioned such that the carboxylate lies near amino acids Y106 and Y341, at the opening of the cyclooxygenase channel [16]. We therefore introduced point mutations to Y341 and its vicinity and explored the effect on the formation of the COX-2 fragment. As depicted in Fig. 2E-F, a double mutation in Y341A/H342A caused a marked reduction in the appearance of the fragment in response to AA, and an additional mutation at G340 (G340A/Y341A/H342A) prevented it altogether. These mutations also caused a severe reduction in the catalytic activity of COX-2 as measured by its ability to generate PGE_2 (Fig. 2G). Finally, a COX-2 mutant that binds AA but shows minimal enzymatic activity compared to the native enzyme (G519A) [15], also prevented the appearance of this band (Fig. 2H). Together, these data indicate that AA-mediated formation of the COX-2 fragment requires both productive binding and catalytic processing of AA, as attenuation of AA binding and impairment of catalysis either chemically or genetically prevents its formation.

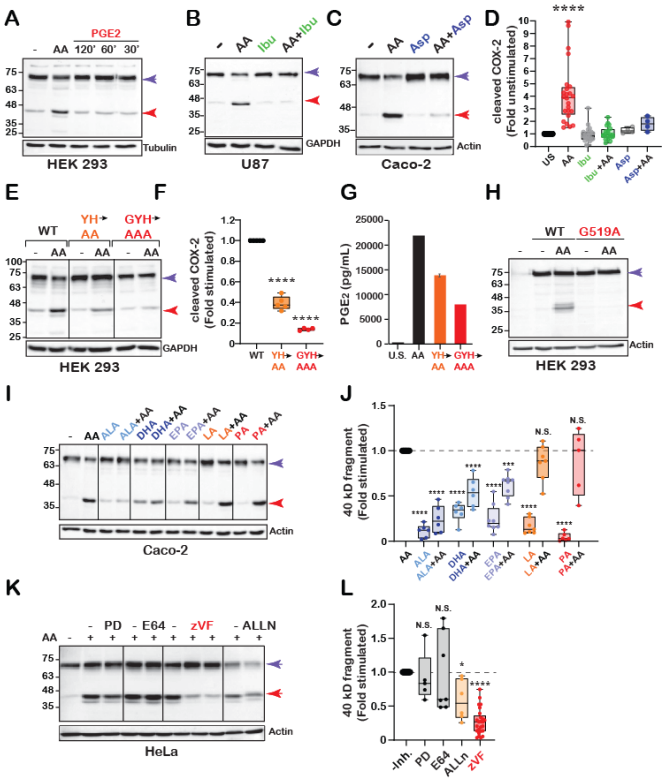

Fig. 2: The appearance of the COX-2 fragment requires enzymatic activity

(A) Western blot of COX-2 expressing HEK 293 cells, treated with either AA or PGE_2 at different time points.

(B) Western blot of U87 cells stimulated with AA in the absence or presence of ibuprofen (Ibu).

(C) Western blot of Caco-2 cells stimulated with AA in the absence or presence of aspirin (Asp).

(D) Box and whisker plot illustrating the quantification of average changes in the levels of the COX-2 fragment in response to ibuprofen. A total of n=24 consisting of data obtained from U87 (n=4), A549 (n=6), HeLa (n=2), RAW 264.7 (n=3), Caco-2 (n=5), HCT-116 (n=4) for ibuprofen or aspirin (Caco-2, n=4).

(E) Western blot depicting the response of HEK 293 cells expressing either WT, double mutation (Y341A/H342A, orange), or triple mutation (G340A/Y341A/H342A) COX-2 to AA stimulation.

(F) Quantification of the COX-2 fragment levels in (E) after normalization by GAPDH (n=4).

(G) Quantification of PGE_2 levels produced by stimulation of HEK 293 cells expressing WT and COX-2 mutants (n=2).

(H) Western blot depicting the response of HEK 293 cells expressing WT or G519A COX-2 to AA stimulation.

(I) Representative western blot of Caco-2 cells treated with different fatty acids (100 μM each) 30 min before AA stimulation.

(J) Quantification of COX-2 fragment levels in (I) after normalization by actin. ALA (n=6), DHA (n=6), EPA (n=8), LA (n=7), PA (n=5).

(K) Representative blots of HeLa cells treated with the protease inhibitors PD150606 (PD, 50 μM), E64D (10 μM), zVF (50 and 100 μM), and ALLN (10 μM) overnight, before AA stimulation.

(L) Quantification of COX-2 fragment levels in (K) after normalization by GAPDH or actin in response following treatment with protease inhibitors. PD150606 (n=5), E64 (n=7), ALLN (n=6), zVF (n=25).

Statistical analysis was assessed by One-way ANOVA ****$p < 0.0001$, with Dunnett's multiple comparisons post-test.

The rate of AA catalysis by COX-2 was previously shown to be differentially modulated by the binding of both substrate- and non-substrate fatty acids (FAs) [4,6,9]. To determine if FAs also affect the appearance of the COX-2 fragment, we treated COX-2-expressing cells with saturated and unsaturated (ω3, ω6) FAs before AA stimulation. As depicted in Fig. 2I-J, the ω3 FAs dihomo-γ linoleic acid (DHA, 22:6ω3), α linolenic acid (ALA, 18:3ω3), and eicosapentaenoic acid (EPA, 20:5ω3) all caused a slight increase in the formation of the fragment when applied alone. Remarkably, when applied before stimulation with AA, all three FAs severely reduced the appearance of the COX-2 fragment. In contrast, linoleic acid (LA, 18:2ω6) or palmitic acid (PA, 16:0) had no effect on its appearance following activation. These findings suggest that the appearance of a COX-2 fragment following enzymatic activity is a physiological event the levels of which are affected by the content of FAs present.

Our data so far indicates that the appearance of the COX-2 fragment is a post-translational event that may be carried out by proteolysis. Previous studies had indicated that cleavage of the full-length (F.L.) COX-2 is reduced by different cysteine protease inhibitors, among which calpain inhibitors had the strongest effect [17,18]. To test whether calpain, a calcium-dependent cysteine protease is also involved in AA-mediated generation of the COX-2 fragment, we tested its formation in the presence of an array of general cysteine protease inhibitors and selective calpain inhibitors. As shown in Fig. 2K, E64 (a broad-spectrum cysteine protease inhibitor) [18] and PD150606 (a selective calpain inhibitor) [19] did not affect the AA-mediated formation of the COX-2 fragment. Application of ALLN (calpain inhibitor I) reduced the appearance of the fragment by approximately 60 %, and Z-Val Phe-OH (zVF, Calpain III), a potent cell-permeable calpain I and II, had the most profound effect, inhibiting approximately 75 % of cleavage (Fig. 2L).

Identification and ectopic expression of COX-2 fragments

Given the above findings, we next sought to identify AA-mediated cleavage points in COX-2. For this purpose, we stimulated RAW 264.7 cells with LPS to induce COX-2 expression, followed by exposure to AA to induce cleavage. Samples were then separated by SDS-PAGE, and proteins were extracted and subjected to Liquid Chromatography with tandem mass spectrometry (LC-MS/MS) analysis. Total lysates from the same experiments were analyzed by western blot in parallel, to confirm the appearance of the fragment. Probing the membranes with anti-COX-2 against the N-terminal of COX-2 identified the F.L. COX-2 as well as the additional ~40 kD band that was detected in the other cell lines (Fig. 3A and Fig. 1). The use of an additional antibody directed against the C-terminal of COX-2 detected the F.L. form and a prominent band of ~ 30 kD (Fig. 3B). Given that the size of F.L. COX-2 is ~72 kD, these results suggest

that at least one cleavage point is present roughly in the middle of the protein, one which gives rise to two complementary fragments of ~40 and ~30 kD.

Analysis of three independent LC-MS/MS experiments yielded seven putative cleavage points, four of which occurred at amino acids that are identical to those of human COX-2 (177, 213, 338 and 341, Fig. 3C). Interestingly, the estimated mass of two cleavage products that were very close to one another (positions 338-339 and 341-342, marked in red) were ~40 kD (1-338/1-341) and 30 kD (339-604 and 342-604), which is similar to the estimated mass of the fragments obtained by western blot (Fig. 3A-B). To confirm this, we ectopically expressed one of the putative fragments (1-338, NT1 herein) in HEK 293 cells, and ran the sample alongside a sample of AA-stimulated COX-2. As shown in Fig. 3D, NT1 migrated to the same distance as the 40 kD COX-2 immunoreactive fragment that appears following AA stimulation.

Our data show that cleavage of COX-2 is a post-translational event that must be preceded by enzymatic activity (Fig. 2). Therefore, studying the possible effects of the AA-dependent fragments cannot be done simply by activation of COX-2 with AA, since this will yield a mixed response of PG-dependent and independent effects. To separate between the two, we cloned the sequences of two pairs of putative COX-2 fragments that complement each other to the size of F.L. COX-2: NT1 (amino acids, aa 1-338, Fig. 3D) and its complementary CT1 (aa 339-604) and NT2 (aa 1-341) and its complementary CT2 (aa 342-604), and expressed each one ectopically. We then confirmed that in contrast to F.L. COX-2, none of these fragments can generate PGE_2, indicating that they lack enzymatic activity (Fig. 3E).

The COX-2 homodimer is associated with the ER and nuclear membranes by four amphipathic helices of its membrane binding domain (MBD). These chains surround the opening of the cyclooxygenase channel through which AA enters the COX site [20]. Since amino acids 338-342 are located near the opening of the cyclooxygenase channel [16], we hypothesized that loss of the MBD motif due to cleavage may result in changes in the cellular localization of some of the fragments compared to that of the F.L. protein. To test this, we examined the cellular localization of the F.L. COX-2 and each of the putative fragments. As depicted in Fig. 3F-G, F.L. COX-2 appears almost entirely in the non-nuclear fractions (97%) as indicated by staining with antibodies against the N- and C-termini (left lane of all images in Fig. 3F). The same is true for fragment NT2 (99%) but not for NT1, 32% of which is found in nuclear fractions (Fig. 3F top left panel and Fig. 3G). In marked contrast to F.L. and NT fragments, both CT1 and CT2 localize primarily to the nuclear fractions (90% and 73%, respectively, Fig. 3F-G).

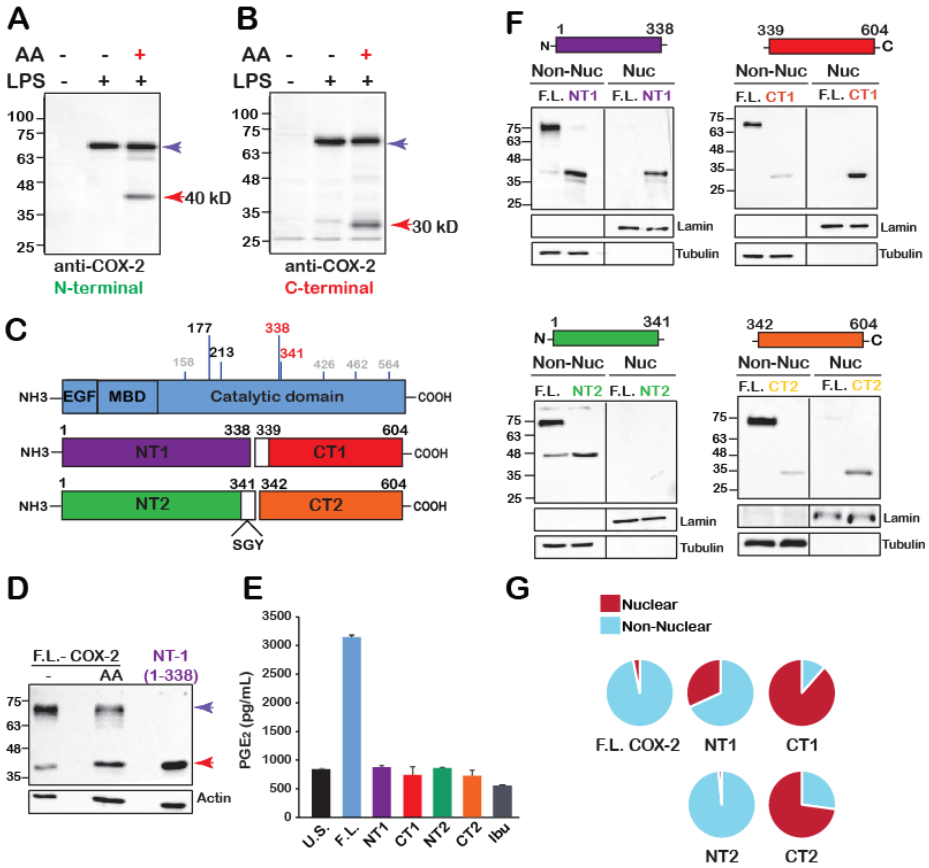

Fig. 3: Identification and ectopic expression of COX-2 fragments

(A-B) Western blots of RAW 264.7 cells stimulated overnight with LPS before exposure to AA using antibodies against the amino- (A) and carboxy- (B) termini of COX-2.

(C) Schematic depiction of the cleavage sites identified by LC-MS/MS in RAW 264.7 cells and the overlapping amino acids in homo sapiens (Top drawing). Schematic representations of the putative cleavage products that were introduced into cells. NT1=1-338, CT1=339-604 (middle drawing), and NT2=1-341 and CT2=342-604 (bottom drawing).

(D) Western blot depicting NT1 relative to AA-stimulated COX-2 in HEK 293 cells.

(E) Quantification of PGE_2 levels produced by HEK 293 cells expressing WT COX-2 or the different fragments. U.S. represents cells expressing WT COX-2 without stimulation, and Ibu represents cells treated with ibuprofen for 30 min before AA stimulation, (n=2).

(F) Representative immunoblots of nuclear (Nuc) and non-nuclear (Non-Nuc) fractions of HEK293 cells expressing F.L. COX-2 or each of the four fragments.

(G) Pie charts quantifications of COX-2 or fragments after normalization of nuclear fractions to lamin B and non-nuclear fractions to tubulin. NT1 (n=7), CT1 (n=5), NT2 (n=4), CT2 (n=7).

CT1-COX-2 reduces mitochondrial function and increases lactate production

The marked differences in localization of CT1 and CT2 compared to F.L. COX-2 led us to postulate that they may differentially affect cellular pathways by altering gene expression. To test this hypothesis, we sequenced the transcriptomes of control (untransfected, UT) and cells with stable expression of CT1 or CT2. A principal component analysis (PCA) of the resulting gene-level expression measurements revealed that both CT1 and CT2 exhibit different transcriptomic profiles compared to the control cells as well as to each other (Fig. 4A). Analysis of the RNA-seq data identified a total of 1852 genes that were differentially expressed (DE) between CT1 and CT2, (1008 genes, 54% upregulated (Table S1) and 844, 46% downregulated (Table S2); Benjamini-Hochberg adjusted $p<0.05$) (Fig. 4B), even though the two CT fragments differ only in the additional three N-terminal amino acids of CT1. To select for effects that were specific to the longer CT1 fragment that was almost exclusively found in nuclear fractions, we performed an additional filtering step for genes that also changed between CT2 and UT cells, which resulted in a list of 608 genes that were uniquely affected by the expression of CT1, 295 (49%) of which were upregulated (Table S3) and 313 (51%) were downregulated (Benjamini-Hochberg adjusted $p<0.05$) (Tables S4).

We next used Metascape [21] to identify the pathways that are enriched among the DE genes (Tables S3 and S4). This analysis revealed a significant enrichment of genes belonging to cellular aerobic respiration among the genes upregulated in CT1-expressing cells (e.g. Electron transport chain OXPHOS system in mitochondria, WP111, $q = 2.0*10^{-7}$; Respiratory Electron Transport, R-HAS-163200, $q = 1.5*10^{-6}$; aerobic respiration, GO: 0009060, $q = 1.1*10^{-4}$) (Fig. 4C, Table S5). The genes downregulated in CT1-expressing cells showed less significant enrichment for functional groups (Figure S1, Table S6). Application of the STRING database [22] on all DE genes revealed a network of 17 genes belonging to the electron transport chain (WP111 Electron transport chain OXPHOS system in mitochondria, Fig. 4D). Interestingly, the effect on the electron transport chain was mixed: genes belonging to complex I (NADH-Ubiquinone oxidoreductase) were all elevated, whereas those belonging to complex II and V (Succinate-Ubiquinone oxidoreductase, and ATP synthase, respectively) were downregulated. Genes belonging to complex IV showed a mixed effect where some genes were upregulated while others were downregulated (Fig. 4D).

Based on the results of the RNA-seq analysis, we next measured the effect of all COX-2 fragments on mitochondrial membrane potential using tetramethylrhodamine ethyl ester (TMRE), as described [23]. Remarkably, only cells that expressed CT1 presented a significant reduction in the levels of high-membrane potential mitochondria (Fig. 4E). Reduced aerobic respiration can potentially lead to the

generation of ATP by the anaerobic glycolysis pathway which leads to the production of lactate. We therefore measured lactate levels in the supernatant of cells expressing the four fragments (Fig 4F). The data depicted in Fig. 4F confirmed that compared to cells expressing F.L. COX-2 only cells that expressed CT1 exhibited elevated lactate levels.

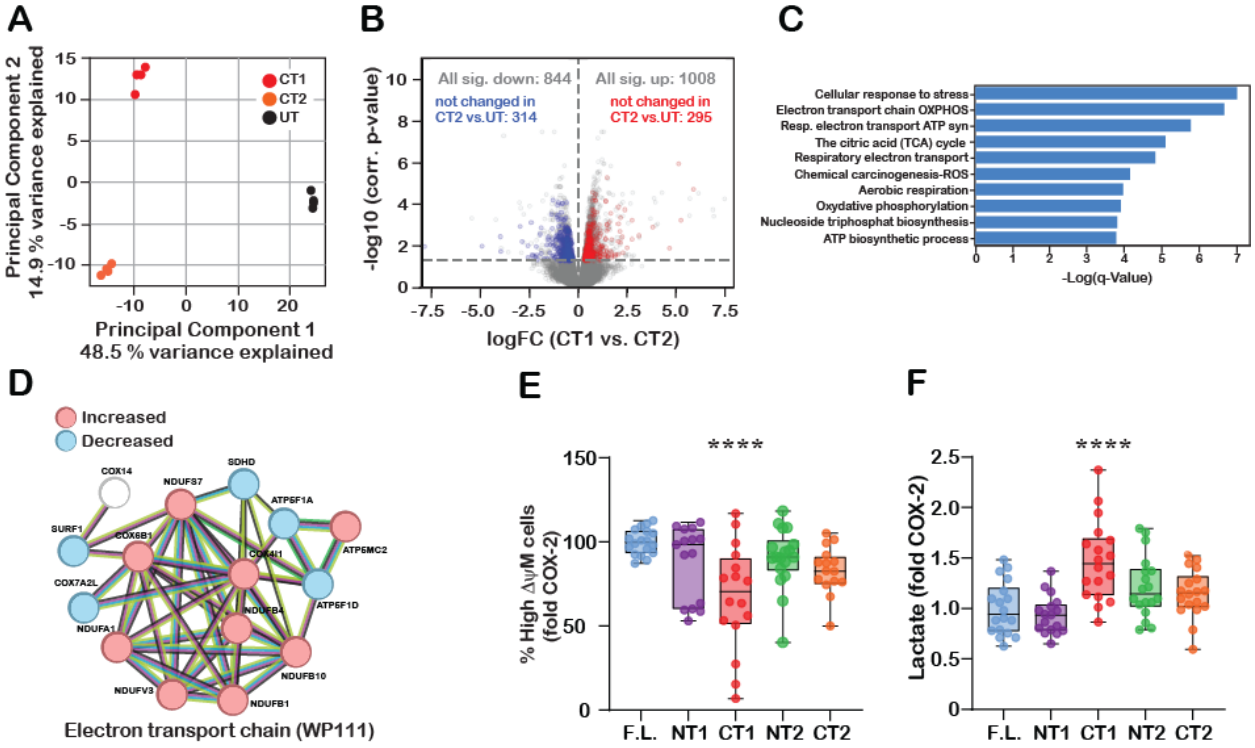

Fig. 4: CT1-COX-2 reduces mitochondrial function and increases lactate production

(A) Scatter plot showing the first two principal components from a PCA based on normalized and standardized expression values of all genes covered by at least 10 reads in all samples.

(B) Volcano plot depicting the differential expression of genes between CT1- and CT2-expressing cells. The horizontal dashed line indicates the significance cutoff (adjusted p-value<0.05). Red and blue data points indicate genes that change between CT1- and CT2-expressing cells but do not exhibit a significant increase or decrease in CT2-expressing compared to control cells.

(C) Top 10 most significantly enriched functional groups (as determined using Metascape) among the upregulated genes in CT1- compared to CT2-expressing cells, which showed no significant change between CT2-expressing and control cells.

(D) STRING analysis of a DE gene set showing a minimum interaction score of highest confidence (0.9).

(E) Box and whiskers plot describing the effect of COX-2 fragments on mitochondrial function, normalized to WT COX-2: F.L. COX-2 (n=19), NT1 (n=15), CT1 (n=16), NT2 (n=16), CT2 (n=15). One-Way ANOVA, *** p<0.001 vs. COX-2 (Dunnett's multiple comparisons post-test).

(F) Box and whiskers plot describing the effect of COX-2 fragments on lactate production, normalized to WT COX-2: F.L. COX-2 (n=18), NT1 (n=17), CT1 (n=18), NT2 (n=18) CT2 (n=18). One-Way ANOVA, *** p<0.001, 001 vs. COX-2 (Dunnett's multiple comparisons post-test).

Discussion

The main finding of the present study is that following AA-induced catalytic activity, COX-2 undergoes limited proteolysis, and at least one of the resulting fragments affects aerobic respiration. Hence, we propose that COX-2 fulfills two different roles in the cell. The first is its undisputed role as a central enzyme that generates soluble ligands of inflammation, and the second is a PG-independent role that is mediated through interactions of COX-2 fragments with different cellular pathways. A non-catalytic role has been previously ascribed to COX-2 in a series of studies showing that it inhibits the function of the tumor suppressor p53 through a direct interaction between the two proteins [24,25]. In contrast to our findings, the effect of COX-2 on p53 was found to occur without stimulation. Furthermore, p53 interacts with the non-catalytic regions of COX-2 (amino acids 1-126), while we identify effects that are mediated by regions of the catalytic domain of the protein (amino acids 339-604). Nonetheless, both studies complement each other by supporting additional cellular functions for COX-2, beyond those obtained by generation of PGs.

The structure and function of the COX-2 enzyme have been studied in-depth, providing detailed information regarding the kinetics of AA catalysis, and interactions of FAs and COX inhibitors with its catalytic and allosteric sites [6,7,9,15]. One of the most important properties of COX-2 is that its ability to generate PGs is limited by self-induced suicide inactivation occurring within seconds of activation [26]. In terms of its expression, COX-2 is an immediate-early gene that is rapidly and massively upregulated to meet the high demand for PGs during inflammation, and elevated COX-2 levels are hallmarks of chronic inflammation and many types of malignancies [27]. Whereas the majority of the high-volume literature concerning COX-2 focuses on its transcriptional regulation [1] and the pharmacological means to inhibit its enzymatic activity [28], very little is known about pathways that clear COX-2 from the cell. This question is of particular importance given the rapid inactivation of COX-2 by its catalysis products. Previous studies have indicated that in the absence of AA, COX-2 is degraded in the cellular proteasome, but that the activated protein is no longer degraded there [11,12]. In a subsequent study, we demonstrated that part of the substrate-inactivated protein is discarded from the cells by exosomes [13], and we now further bridge the gap by showing that COX-2 is also subjected to controlled cleavage, which mediates additional cellular functions.

COX-2 was previously shown to undergo proteolysis into discrete fragments following exposure of human synovial fibroblasts to pro-inflammatory cytokines [18]. Using an anti-pan-human COX-2 with an undesclosed epitope, the researchers identified four COX-2 fragments, two of which are similar to those identified by us (44-42 and 34-36 kD). Using the same antibody against the C-terminus of COX-2 as we

have (Fig. 3B), they also identified a fragment of 30 kD, which like CT1 and CT2 (Fig. 3G), localizes to nuclear and mitochondrial-lysosomal fractions. The similarity between the sizes of fragments in both studies is probably because the cytokine IL-1β causes AA release [29], which is comparable to the application of AA directly onto the cells. However, while Mancini et al ascribe a role for proteolysis in protein maturation, we show that the putative fragments completely lack enzymatic activity, thus suggesting that they affect the cell in a PG-independent manner. These results are supported by our previously published finding that COX-2 which lacks the EGF and MBD domains (ΔCOX-2) is catalytically inactive [30].

The search for protease/s that cleave COX-2 is challenging. Whereas the F.L. unstimulated COX-2 is degraded in the proteasome, it no longer does so after catalytic activity [12]. Since the putative cleavage site in our study lies at the surface of the protein [16], and given earlier indications [17,18], we examined calpain as a possible candidate for COX-2 proteolysis. Calpain was shown to degrade COX-2 in vitro [17], and indeed calpain inhibitors such as the calpain III inhibitor zVF significantly decreased the appearance of the 40 kD fragment (Fig. 2K-L). However, zVF also targets γ-secretase [31], and even though it inhibited the majority of cleavage, it did not obliterate it, even in the presence of a cycloheximide that inhibits *de novo* synthesis (not shown). Therefore, the identity of the protease/s that cleave COX-2 is yet to be determined.

In summary, we propose that COX-2 fulfills two different cellular functions that occur in two waves. The first wave is through its enzymatic action and the generation of PGs that activate G protein-coupled receptors and relay their signals through soluble second messengers. The second wave arises from the secession of catalytic activity which leads to the secretion of part of the F.L. protein by exocytosis [13] as well as to its controlled proteolysis. The products of proteolysis can now migrate to different cellular compartments where they affect cellular function in mechanisms that are PG-independent. Characterization of these pathways and discovery of additional functions of COX-2 fragments will further our understanding of the complex role of COX-2 in pathologies such as proliferative diseases and chronic inflammation and may help identify novel targets for intervention against its components.

Acknowledgments

The authors wish to thank Dr. Sagie Schif-Zuck from the Flow Cytometry Service Unit, University of Haifa for assistance with the flow cytometry analyses, and Dr. Maya Lalzar from the Bioinformatics Services

Unit, University of Haifa, for assistance with transcriptome data. This work was supported by the Israel Science Foundation personal grant to L.B.H. (1445/14 and 2240/19).

Author contributions

Conceptualization, S.T and L.B-H; Methodology, S.T. O.K, and L.B-H; Investigation, L.H-B., S.T., R.S-E, A.A., O.E., M.M., L. B-H.; Writing-Original draft, L.B-H; Writing-Review & Editing, L.B-H, M.M.; Funding Acquisition, L. B-H.; Resources, M.M., L.B-H., Supervision, L.B-H.

Declaration of Interests

The authors declare no competing interests.

STAR Methods

REAGENT or RESOURCE	SOURCE	IDENTIFIER
Antibodies		
COX-2 Rabbit monoclonal Ab	Cell Signaling Technology	12282 (H5H5) XP
COX-2 (C-20) goat polyclonal Ab	Santa Cruz Biotechnology Inc.	SC-1745
Beta Actin rabbit polyclonal Ab	Abcam	115777
GAPDH (D4C6R) monoclonal Ab	Cell Signaling Technology	
Lamin B	Cell Signaling Technology	CST-13435
Tubulin	Abcam	6160
Horseradish peroxidase-conjugated goat anti-rabbit IgG	Jackson ImmunoResearch Laboratories	111-035-144
Horseradish peroxidase-conjugated goat anti-mouse IgG	Jackson ImmunoResearch Laboratories	115-035-003
Peroxidase AffiniPure™ Bovine Anti-Goat IgG (H+L)	Jackson ImmunoResearch Laboratories	805-035-180
Bacterial and virus strains		
Biological samples		
Colorectal biopsies (human)	HaEmek Medical Center	Ha'Emek Medical Center- 0049–19
Chemicals, peptides, and recombinant proteins		
Arachidonic acid	Cayman Chemical	90010
Aspirin	Cayman Chemical	70260
Alpha linolenic acid	Cayman Chemical	90210
Beta-Nicotinamide adenine dinucleotide hydrate	Sigma-Aldrich	N7004
BLUEYE prestained protein ladder	BIO-HELIX	IMPM007
Calpain inhibitor I (ALLN)	Sigma-Aldrich	11086090001
Calpain inhibitor III -zvf	Sigma-Aldrich	208722
Complete(TM) Protease Inhibitor Cocktail	Sigma Aldrich	11697498001
Docosahexaenoic Acid (DHA)	Cayman Chemical	90310

DAPT	Cayman Chemical	13197
E64	Sigma Aldrich	E3132
Eicosapentaenoic Acid (sodium salt)	Cayman Chemical	21908-5
Hygromycin B	Sigma Aldrich	H3274
Ibuprofen	Cayman Chemical	16793
Imperial™ Protein Stain Coomassie dye	Rhenium	24615
Iodonitrotetrazolium chloride	Sigma-Aldrich	I8377
L-lactate dehydrogenase (LDHA)	Sigma-Aldrich	10127230001
L-lactate (sodium)	Sigma-Aldrich	PHR1113
Lipopolysaccharide (LPS)	Sigma Aldrich	L6529
Linoleic acid	Sigma-Aldrich	L1012
Methoxy-PMS	BioTag	HY-D0937
Palmitic Acid	Cayman Chemical	10006627
PD 15606	Sigma Aldrich	D5946
PolyJet In Vitro DNA Transfection Reagent	SingaGen	SL100688
Prostaglandin E2	Cayman Chemical	14010
Protein Assay Dye Reagent Concentrate	Bio-Rad	5000006
Protein A/G PLUS-Agarose	Santa Cruz Biotechnology	SC-2003
RNase-ExitusPlus	Satorius	01-897-1B
TMRE-Mitochondrial Membrane Potential	Abcam	ab113852
Critical commercial assays		
Prostaglandin E2 Parameter Assay Kit	R&D Systems, Inc.	KGE004B
QuikChange Lightning Site-Directed Mutagenesis Kit	Agilent	210519
PRESTO™ MINI PLASMID KIT	Hylabs	IMPDH100
Deposited data		
Experimental models: Cell lines		
A549	Sheba	Gift Amir Onn
Caco-2	ATCC	HTB-37
HCT-116	ATCC	CCL-247
HEK 293	Technion Ins, Israel	Gift Dina Ron
HeLa	ATCC	CRM-CCL-2
MCF10A	Technion Ins, Israel	Gift Israel Vlodavsky
RAW 264.7	ATCC	TIB-71
U87	ATCC	HTB-14
Experimental models: Organisms/strains		
Oligonucleotides		
Recombinant DNA		
Y341A H342A human cox2 (in pcDNA5/FRT/TO)		
COX2 G340A Y341A H342A human cox2 (in pcDNA5/FRT/TO)		
Software and algorithms		
GraphPad Prism 10		
Adobe Illustrator CS5.1		
Adobe Photoshop CS5.1		
ImageQant TL 1D v8.1		
EndNote X7		

Other		
Quick-RNA™ Miniprep Plus Kit	Zymo	ZR-R1058
Nitrocellulose blotting membrane- 0.45 μm	Tamar	980045
PureYield™ Plasmid Midiprep System	Promega	A2492
NEBNext Ultra RNA library Prep kit for Illumina	Thermo Fischer Scientific	E75030L

Patient biopsies

Human colon biopsies were obtained from individuals diagnosed and operated on at Ha'Emek Medical Center, Afula Israel. All patients were diagnosed with adenocarcinoma of the colon or rectum, with tumors that were graded at least B2 or higher. Biopsies were obtained during surgery upon written consent from patients according to the Helsinki regulations (Ha'Emek Medical Center- 0049–19) and flash-frozen in liquid N_2 pending analysis. For identification of COX-2 expression patterns were processed exactly using the same samples as we have before [30]. 150 μg of total tissue lysates were analyzed.

Cell culture and transfection

A549 lung cancer cells were grown in RPMI. RAW 264.7, U87, HeLa, HEK 293, HCT-116, and Caco-2 were grown in DMEM. All media was supplemented with 10% heat-inactivated fetal bovine serum, 1% pyruvate, 100 μg/mL streptomycin, and 100 U/ml penicillin. MCF-10A cells were grown in DMEM/F12 exactly as described [32].

Transient transfections were carried out in sub-confluent monolayers (70-80%) using PolyJet (SignaGen Laboratories) at a ratio of 1:3 cDNA: PolyJet, according to the manufacturer's instructions. HEK293-derived cell lines stably expressing native or fragment COX-2 constructs were generated using hygromycin selection (200 μg/mL medium) for 9 days. The resulting colonies were tested for the presence of each fragment by western blot.

Cell stimulation, processing, and Immunoblotting

Unless otherwise indicated, all stimulations with AA were at 50 μM for 30 min. All fatty acids used in the study were applied at 100 μM for 30 min before AA stimulation, as were the inhibitors ibuprofen (200 μM) and aspirin (100 μM). Treatments with the different protease inhibitors were applied for 18-24 h at the following concentrations: PD15606 (50 μM), ALLN (10 μM), E64 (10 μM), zVF (50 or 100 μM). Monolayers were washed twice with ice-cold PBS and lysed in RIPA/SDS buffer (50 mM Tris pH- 8, 150 mM NaCl, 5 mM EDTA, 1% v/v NP-40, 0.5%, 0.5% w/v deoxycholic acid, 0.1% w/v SDS, 10 mM NaF, 10 mM sodium-pyro-phosphate and Complete Protease Inhibitor cocktail tablets with 0.1 mM PMSF) and process exactly as we have done before [30]. Subcellular fractionation was done using the Rapid, Efficient

And Practical (REAP) method [33]. The protocol was carried out exactly as described, except for the addition of Complete and 0.1 mM PMSF to the lysis buffer. 40 μg of total protein lysates were used in all blots. Nitrocellulose membranes containing the immuno-complexes or total cell lysate proteins were incubated with primary antibodies at a dilution of 1:500–1000. Proteins were visualized by a WesternBright ECL (Advansta) and quantified using the Amersham Imager 600 (GE) and quantified using ImageQant TL 1D v8.1 software.

Immunoprecipitation and mass spectrometry

7 x 10^6 RAW 264.7 cells were grown in 15 cm dishes and stimulated overnight with 100 ng/mL LPS, followed by a 30-minute stimulation with 50 μM AA. The reaction was terminated by two subsequent washes with ice-cold PBS and lysis in 0.5 mL RIPA/SDS buffer. Samples were centrifuged at 14,000 × g at 4 °C for 10 min, the supernatants were collected, and protein levels were determined. 100 μg of the lysates were used for total protein assessment. 3-3.5 mg protein were used for IP experiments. Samples were pre-cleared with 20 μl of protein A/G beads for 60 min, centrifuged again at 14,000 × g at 4 °C for 2 min and the remaining supernatant was used for overnight immunoprecipitation with 2 mg goat polyclonal anti-COX-2 (Santa Cruz Biotechnology, SC-1745) and 30 μl protein A/G beads with continuous rotation at 4 °C. After three subsequent washes with 0.75 mL RIP/SDS, lysates were separated by a 10% sodium dodecyl sulfate (SDS) polyacrylamide gel. The entire protein lane of each sample was cut into three horizontal gel pieces and processed by in-gel trypsin digestion procedure as described before [34], followed by peptides desalting using C18 StageTip [35]. Whole proteome and activity-guided proteasome profiling samples were analyzed using a Q-Exactive Plus mass spectrometer (Thermo Fisher) coupled to Easy nLC 1000 or Dionex (Thermo Fisher). The peptides were resolved by reverse-phase chromatography on 0.075 × 180 mm fused silica capillaries (J&W) packed with Reprosil reversed-phase material (Dr. Maisch; GmbH, Germany). Peptides were eluted with a linear gradient of 6–28% acetonitrile 0.1% formic acid for 60 min followed by a 15 min gradient of 28–95% acetonitrile 0.1% formic acid and a 15 min wash at 95% acetonitrile with 0.1% formic acid in water (at flow rates of 0.15-0.2 μL/min).

The MS analysis was performed in positive mode using a range of m/z 300–1800, resolution of 70,000 for MS1 and 17,500 for MS2, using, repetitively, full MS scan followed by HCD of the 10 most dominant ions selected from the first MS scan with an isolation window of 1.8 m/z. Other settings used were as follows: a dynamic exclusion of 20 seconds, NCE=27, minimum AGC target=8x10^3, and intensity threshold=1.3x10^5. Data analysis was done using MSFragger version 4.0 [36] via FragPipe version 21.1 (https://fragpipe.nesvilab.org/). In all searches, the raw files were searched against the Uniprot

Mouse/Human proteome (Downloaded on Feb 2024 and includes 54940/ 20413 protein sequences, respectively). MSFargger searches were performed by using semi-tryptic digestion. Search criteria included precursor and fragments tolerance of 20 ppm with oxidation of methionine, and protein N-terminal acetylation set as variable modifications.

COX-2 activity measurements

The media of 3×10^5 transfected HEK 293 in 6-well dishes was siphoned, and the cells were washed twice with warm PBS and incubated in 1 mL of serum-free DMEM with AA for 30min. In the FA experiments, cells were treated with the different FAs (100 μM each) or with the appropriate vehicle for 30 min, followed by an additional 30 min with 50 μM AA. At the end of the experiment, the supernatant was collected and the levels of PGE_2 were analyzed using the Prostaglandin E_2 Assay (R&D Systems), according to the manufacturer's instructions.

Mitochondrial activity measurements

0.05×10^6 HEK 293 cells were seeded in 12-well dishes and transfected with 0.75 μg F.L. COX-2 or fragment cDNA. 72h post-transfection the ΔΨm was measured as previously described [23]. Briefly, the cells were dissociated with trypsin and washed twice with ice-cold 0.2% BSA in PBS. After centrifugation for 5 min at 1500 rpm, the cells were incubated in the dark at 37 °C, for 20 min with Mitochondrial Tracker Green (Ex/Em 490/516) for general mitochondria staining, and TMRE for mitochondrial membrane potential (Ex/Em 549/575 nm). After an additional wash with 1 mL of 0.2% BSA, the cells were resuspended in 300 μl 0.2% BSA and immediately analyzed by the BD FACSCanto II flow cytometer with DACSDiva software (BD Biosciences). Gates were set to exclude necrotic cells and cellular debris and the fluorescence intensity of events within the gated regions was quantified. Data were collected from 10000 events for each sample. The relative percentage of cells with high Δψm was calculated as % high Δψm of total (high Δψm + low Δψm).

L-Lactate level measurements

L-lactate levels were measured by a colorimetric assay of lactate dehydrogenase (LDH) activity 0.3×10^6 HEK 293 cells were seeded in 6-well dishes and transfected with 1 μg cDNA of F.L. COX-2 or fragments in 1 mL complete DMEM media. 72h post-transfection the external media of the cells was collected and probed for the presence of lactate exactly according to the step-by-step protocol in https://www.protocols.io/view/colorimetric-determination-of-l-lactate-in-superna-dm6gpj9j5gzp/v1. Briefly, 50 μl of sample supernatants were placed in a flat-bottom 96-well dish (in triplicates) followed by the addition of 50 μl Assay buffer (200 mM Tris-Base, pH=8.2, 2.2 mg/mL β-NAD, 0.5 mg/mL INT, 1

μg/mL L-LDH, 6 μg/mL 1-Methoxy-PMS) and incubated for 1 h at room temperature in the dark. The reaction was terminated by the addition of 50 μl Acetic Acid (1 M) and the absorbance was measured at 490 nm-Ref 650 nm with a microplate absorbance reader. If lactate concentration was above that of the standard curve, samples were diluted in DMEM.

Transcriptome analyses and statistics

Total RNA was prepared from four biological replicates using the Quick-RNA MiniPrep kit (Cat. # ZR-R10554, Zymo Research). Library preparation was performed using NEBNext Ultra RNA library Prep kit for Illumina (Cat. # E7530L, Thermo Fischer Scientific, Waltham, MA USA), according to the manufacturer's protocol. Sequencing (single-read, 50bp) was carried out using the Illumina HiSeq 2500 at the TGC-Technion Genome Center (Technion, Haifa, Israel). Trimming of poly-A and poly-G leftovers was done using the PRINSEQ tool (https://edwards.sdsu.edu/cgi-bin/prinseq/prinseq.cgi) removing reads with more than 58% of A or G in twain with a 3' tail filter (poly-A) of more than 8 bases. Qualified reads were later trimmed for adaptors and low-quality reads using Trimmomatic (v0.39; http://www.usadellab.org/cms/index.php?page=trimmomatic). In addition, reads were clipped to a size between 40-60 bases for optimal mapping. Gene expression levels were quantified using Htseq-count (0.6.1-py2.7) and filtered for genes covered by at least 10 reads in all samples. Differential expression was analyzed using EdgeR (3.2.4). P-values were corrected for multiple testing using the Benjamini-Hochberg method, and differential expression was considered significant for adjusted *P*-value < 0.05. The differentially expressed (DE) genes were subjected to gene-set enrichment analysis using Metascape (accessed March 2024 [21]). Cutoff for significant enrichment was adjusted for multiple testing (Benjamini Hochberg) and the resulting q-values are reported (Tables S5 and S6).

Statistical Analysis

Statistical analyses were done using the GraphPad Prism Software. Unless otherwise stated, statistical significance was determined by one-way ANOVA. Post-hoc analysis was performed with Dunnett's multiple comparisons post-test when appropriate. P values < 0.05 were considered significant.

References

1 Kang, Y. J., Mbonye, U. R., DeLong, C. J., Wada, M. & Smith, W. L. Regulation of intracellular cyclooxygenase levels by gene transcription and protein degradation. *Prog Lipid Res* **46**, 108-125, doi:S0163-7827(07)00002-1 [pii]10.1016/j.plipres.2007.01.001 (2007).

2 Smith, W. L., DeWitt, D. L. & Garavito, R. M. Cyclooxygenases: structural, cellular, and molecular biology. *Annu Rev Biochem* **69**, 145-182, doi:69/1/145 [pii]10.1146/annurev.biochem.69.1.145 (2000).

3 Marnett, L. J., Rowlinson, S. W., Goodwin, D. C., Kalgutkar, A. S. & Lanzo, C. A. Arachidonic acid oxygenation by COX-1 and COX-2. Mechanisms of catalysis and inhibition. *J Biol Chem* **274**, 22903-22906, doi:10.1074/jbc.274.33.22903 (1999).

4 Dong, L., Vecchio, A. J., Sharma, N. P., Jurban, B. J., Malkowski, M. G. & Smith, W. L. Human Cyclooxygenase-2 Is a Sequence Homodimer That Functions as a Conformational Heterodimer. *Journal of Biological Chemistry* **286**, 19035-19046, doi:10.1074/jbc.M111.231969 (2011).

5 Yuan, C., Rieke, C. J., Rimon, G., Wingerd, B. A. & Smith, W. L. Partnering between monomers of cyclooxygenase-2 homodimers. *Proc Natl Acad Sci U S A* **103**, 6142-6147, doi:0601805103 [pii]10.1073/pnas.0601805103 (2006).

6 Dong, L., Yuan, C., Orlando, B. J., Malkowski, M. G. & Smith, W. L. Fatty Acid Binding to the Allosteric Subunit of Cyclooxygenase-2 Relieves a Tonic Inhibition of the Catalytic Subunit. *Journal of Biological Chemistry* **291**, 25641-25655, doi:10.1074/jbc.M116.757310 (2016).

7 Dong, L., Zou, H. C., Yuan, C., Hong, Y. H., Kuklev, D. V. & Smith, W. L. Different Fatty Acids Compete with Arachidonic Acid for Binding to the Allosteric or Catalytic Subunits of Cyclooxygenases to Regulate Prostanoid Synthesis. *Journal of Biological Chemistry* **291**, 4069-4078, doi:10.1074/jbc.M115.698001 (2016).

8 Rimon, G., Sidhu, R. S., Lauver, D. A., Lee, J. Y., Sharma, N. P., Yuan, C., Frieler, R. A., Trievel, R. C., Lucchesi, B. R. & Smith, W. L. Coxibs interfere with the action of aspirin by binding tightly to one monomer of cyclooxygenase-1. *Proc Natl Acad Sci U S A* **107**, 28-33, doi:0909765106 [pii]10.1073/pnas.0909765106 (2010).

9 Smith, W. L. & Malkowski, M. G. Interactions of fatty acids, nonsteroidal anti-inflammatory drugs, and coxibs with the catalytic and allosteric subunits of cyclooxygenases-1 and-2. *Journal of Biological Chemistry* **294**, 1697-1705, doi:10.1074/jbc.TM118.006295 (2019).

10 Rouzer, C. A. & Marnett, L. J. Mechanism of free radical oxygenation of polyunsaturated fatty acids by cyclooxygenases. *Chem Rev* **103**, 2239-2304, doi:10.1021/cr000068x (2003).

11 Haddad, A., Flint-Ashtamker, G., Minzel, W., Sood, R., Rimon, G. & Barki-Harrington, L. Prostaglandin EP1 receptor down-regulates expression of cyclooxygenase-2 by facilitating its proteasomal degradation. *J Biol Chem* **287**, 17214-17223, doi:M111.304220 [pii]10.1074/jbc.M111.304220 (2012).

12 Mbonye, U. R., Yuan, C., Harris, C. E., Sidhu, R. S., Song, I., Arakawa, T. & Smith, W. L. Two distinct pathways for cyclooxygenase-2 protein degradation. *J Biol Chem* **283**, 8611-8623, doi:M710137200 [pii]10.1074/jbc.M710137200 (2008).

13 Saadi, E., Tal, S. & Barki-Harrington, L. Substrate-inactivated cyclooxygenase-2 is disposed of by exosomes through the ER-Golgi pathway. *Biochem J* **475**, 3141-3151, doi:10.1042/BCJ20180530 (2018).

14 Hartal-Benishay, L. H., Saadi, E., Toubiana, S., Shaked, L., Lalzar, M., Abu Hatoum, O., Tal, S., Selig, S. & Barki-Harrington, L. MBTPS1 regulates proliferation of colorectal cancer primarily through its action on sterol regulatory element-binding proteins. *Front Oncol* **12**, 1004014, doi:10.3389/fonc.2022.1004014 (2022).

15 Rowlinson, S. W., Crews, B. C., Lanzo, C. A. & Marnett, L. J. The binding of arachidonic acid in the cyclooxygenase active site of mouse prostaglandin endoperoxide synthase-2 (COX-2). A putative L-shaped binding conformation utilizing the top channel region. *J Biol Chem* **274**, 23305-23310 (1999).

16 Malkowski, M. G., Ginell, S. L., Smith, W. L. & Garavito, R. M. The productive conformation of arachidonic acid bound to prostaglandin synthase. *Science* **289**, 1933-1937, doi:10.1126/science.289.5486.1933 (2000).

17 Liu, T., Huang, Y., Likhotvorik, R. I., Keshvara, L. & Hoyt, D. G. Protein Never in Mitosis Gene A Interacting-1 (PIN1) regulates degradation of inducible nitric oxide synthase in endothelial cells. *Am J Physiol Cell Physiol* **295**, C819-827, doi:10.1152/ajpcell.00366.2007 (2008).

18 Mancini, A., Jovanovic, D. V., He, Q. W. & Di Battista, J. A. Site-specific proteolysis of cyclooxygenase-2: a putative step in inflammatory prostaglandin E(2) biosynthesis. *J Cell Biochem* **101**, 425-441, doi:10.1002/jcb.21191 (2007).

19 Wang, K. K. W., Nath, R., Posner, A., Raser, K. J., BurokerKilgore, M., Hajimohammadreza, I., Probert, A. W., Marcoux, F. W., Ye, Q. H., Takano, E., Hatanaka, M., Maki, M., Caner, H., Collins, J. L., Fergus, A., Lee, K. S., Lunney, E. A., Hays, S. J. & Yuen, P. W. An alpha-mercaptoacrylic acid derivative is a selective nonpeptide cell-permeable calpain inhibitor and is neuroprotective. *P Natl Acad Sci USA* **93**, 6687-6692, doi:DOI 10.1073/pnas.93.13.6687 (1996).

20 Spencer, A. G., Thuresson, E., Otto, J. C., Song, I., Smith, T., DeWitt, D. L., Garavito, R. M. & Smith, W. L. The membrane binding domains of prostaglandin endoperoxide H synthases 1 and 2 - Peptide mapping and mutational analysis. *Journal of Biological Chemistry* **274**, 32936-32942, doi:DOI 10.1074/jbc.274.46.32936 (1999).

21 Zhou, Y., Zhou, B., Pache, L., Chang, M., Khodabakhshi, A. H., Tanaseichuk, O., Benner, C. & Chanda, S. K. Metascape provides a biologist-oriented resource for the analysis of systems-level datasets. *Nat Commun* **10**, 1523, doi:10.1038/s41467-019-09234-6 (2019).

22 Szklarczyk, D., Kirsch, R., Koutrouli, M., Nastou, K., Mehryary, F., Hachilif, R., Gable, A. L., Fang, T., Doncheva, N. T., Pyysalo, S., Bork, P., Jensen, L. J. & von Mering, C. The STRING database in 2023: protein-protein association networks and functional enrichment analyses for any sequenced genome of interest. *Nucleic Acids Res* **51**, D638-D646, doi:10.1093/nar/gkac1000 (2023).

23 Monteiro, L. B., Davanzo, G. G., de Aguiar, C. F. & Moraes-Vieira, P. M. M. Using flow cytometry for mitochondrial assays. *MethodsX* **7**, 100938, doi:10.1016/j.mex.2020.100938 (2020).

24 Choi, E. M., Heo, J. I., Oh, J. Y., Kim, Y. M., Ha, K. S., Kim, J. I. & Han, J. A. COX-2 regulates p53 activity and inhibits DNA damage-induced apoptosis. *Biochem Biophys Res Commun* **328**, 1107-1112, doi:10.1016/j.bbrc.2005.01.072 (2005).

25 Choi, E. M., Kim, S. R., Lee, E. J. & Han, J. A. Cyclooxygenase-2 functionally inactivates p53 through a physical interaction with p53. *Biochim Biophys Acta* **1793**, 1354-1365, doi:S0167-4889(09)00151-7 [pii]10.1016/j.bbamcr.2009.05.006 (2009).

26 Smith, W. L. & Song, I. The enzymology of prostaglandin endoperoxide H synthases-1 and -2. *Prostaglandins Other Lipid Mediat* **68-69**, 115-128, doi:10.1016/s0090-6980(02)00025-4 (2002).

27 Koki, A., Khan, N. K., Woerner, B. M., Dannenberg, A. J., Olson, L., Seibert, K., Edwards, D., Hardy, M., Isakson, P. & Masferrer, J. L. Cyclooxygenase-2 in human pathological disease. *Adv Exp Med Biol* **507**, 177-184, doi:10.1007/978-1-4615-0193-0_28 (2002).

28 Ozleyen, A., Yilmaz, Y. B., Donmez, S., Atalay, H. N., Antika, G. & Tumer, T. B. Looking at NSAIDs from a historical perspective and their current status in drug repurposing for cancer treatment and prevention. *J Cancer Res Clin* **149**, 2095-2113, doi:10.1007/s00432-022-04187-8 (2023).

29 Xiao, D. M. & Levine, L. Stimulation of arachidonic acid metabolism: differences in potencies of recombinant human interleukin-1 alpha and interleukin-1 beta on two cell types. *Prostaglandins* **32**, 709-718, doi:10.1016/0090-6980(86)90193-0 (1986).

30 Saadi, E., Sood, R., Dromi, I., Srouji, R., Hatoum, O. A., Tal, S. & Barki-Harrington, L. Limited Proteolysis of Cyclooxygenase-2 Enhances Cell Proliferation. *Int J Mol Sci* **21**, doi:10.3390/ijms21093195 (2020).

31 Higaki, J., Quon, D., Zhong, Z. & Cordell, B. Inhibition of beta-amyloid formation identifies proteolytic precursors and subcellular site of catabolism. *Neuron* **14**, 651-659, doi:10.1016/0896-6273(95)90322-4 (1995).

32 Debnath, J., Muthuswamy, S. K. & Brugge, J. S. Morphogenesis and oncogenesis of MCF-10A mammary epithelial acini grown in three-dimensional basement membrane cultures. *Methods* **30**, 256-268, doi:10.1016/s1046-2023(03)00032-x (2003).

33 Suzuki, K., Bose, P., Leong-Quong, R. Y., Fujita, D. J. & Riabowol, K. REAP: A two minute cell fractionation method. *BMC Res Notes* **3**, 294, doi:1756-0500-3-294 [pii]10.1186/1756-0500-3-294 (2010).

34 Ziv, I., Matiuhin, Y., Kirkpatrick, D. S., Erpapazoglou, Z., Leon, S., Pantazopoulou, M., Kim, W., Gygi, S. P., Haguenauer-Tsapis, R., Reis, N., Glickman, M. H. & Kleifeld, O. A Perturbed Ubiquitin Landscape Distinguishes Between Ubiquitin in Trafficking and in Proteolysis. *Molecular & Cellular Proteomics* **10**, doi:ARTN M111.00975310.1074/mcp.M111.009753 (2011).

35 Rappsilber, J., Mann, M. & Ishihama, Y. Protocol for micro-purification, enrichment, pre-fractionation and storage of peptides for proteomics using StageTips. *Nature Protocols* **2**, 1896-1906, doi:10.1038/nprot.2007.261 (2007).

36 Kong, A. T., Leprevost, F. V., Avtonomov, D. M., Mellacheruvu, D. & Nesvizhskii, A. I. MSFragger: ultrafast and comprehensive peptide identification in mass spectrometry-based proteomics. *Nat Methods* **14**, 513-520, doi:10.1038/nmeth.4256 (2017).